ResearchGate

See discussions, stats, and author profiles for this publication at: https://www.researchgate.net/publication/27714925

Effect of the Nickel Precursor on the Impregnation and Drying of γ-Al2O3 Catalyst Bodies: A UV−Vis and IR Microspectroscopic Study

ARTICLE *in* THE JOURNAL OF PHYSICAL CHEMISTRY C · MAY 2008

Impact Factor: 4.77 · DOI: 10.1021/jp710676v · Source: OAI

CITATIONS
39

READS
94

3 AUTHORS, INCLUDING:

Krijn P. De Jong
Utrecht University
312 PUBLICATIONS **11,520** CITATIONS
SEE PROFILE

Bert M Weckhuysen
Utrecht University
594 PUBLICATIONS **16,362** CITATIONS
SEE PROFILE

Available from: Krijn P. De Jong
Retrieved on: 17 January 2016

THE JOURNAL OF PHYSICAL CHEMISTRY C

Subscriber access provided by Universiteit Utrecht

Article

Effect of the Nickel Precursor on the Impregnation and Drying of □-AlO Catalyst Bodies: A UV–vis and IR Microspectroscopic Study

Leticia Espinosa-Alonso, Krijn P. de Jong, and Bert M. Weckhuysen

J. Phys. Chem. C, **2008**, 112 (18), 7201-7209 • DOI: 10.1021/jp710676v

Downloaded from http://pubs.acs.org on January 12, 2009

More About This Article

Additional resources and features associated with this article are available within the HTML version:

- Supporting Information
- Access to high resolution figures
- Links to articles and content related to this article
- Copyright permission to reproduce figures and/or text from this article

View the Full Text HTML

ACS Publications
High quality. High impact.

The Journal of Physical Chemistry C is published by the American Chemical Society.
1155 Sixteenth Street N.W., Washington, DC 20036

Effect of the Nickel Precursor on the Impregnation and Drying of γ-Al_2O_3 Catalyst Bodies: A UV−vis and IR Microspectroscopic Study

Leticia Espinosa-Alonso, Krijn P. de Jong, and Bert M. Weckhuysen*

Inorganic Chemistry and Catalysis Group, Department of Chemistry, Utrecht University, Sorbonnelaan 16 3584 CA Utrecht, The Netherlands

Received: November 7, 2007; In Final Form: January 21, 2008

The elemental preparation steps of impregnation and drying of Ni/γ-Al_2O_3 catalyst bodies have been studied by combining UV−vis and IR microspectroscopy. The influence of the number of chelating ligands in $[Ni(en)_x(H_2O)_{6-2x}]^{2+}$ precursor complexes (with en = ethylenediamine and $x = 0-3$) has been investigated. UV−vis measurements after impregnation showed that, regardless of the en:Ni^{2+} ratio in the precursor solution, Ni^{2+} was already detected in the core of the pellets 5 min after impregnation. The alumina support did bring about, however, gradients in the nature of the Ni^{2+} species upon first contact with the lowest en:Ni^{2+} ratio solutions, but these gradients disappeared after 30−60 min of impregnation. After 60 min, UV−vis seemed to indicate Ni−O−Al interactions between Ni^{2+} and the support, when water was initially part of the first coordination sphere of Ni^{2+}, which was supported with the results obtained after drying. For dried samples, UV−vis showed a gradient of $[Ni(en)_x(H_2O)_{6-2x}]^{2+}$ inside the pellets, with an en-poor region in the core and an en-rich region in the edges of the catalyst bodies, when $[Ni(en)_3]^{2+}$ or $[Ni(en)_2(H_2O)_4]^{2+}$ were the starting complexes. IR microspectroscopy confirmed these en radial profiles, while EDX measurements showed that an Ni^{2+} egg-shell distribution goes hand-in-hand with an egg-shell distribution of en. The number of en ligands determined the interactions of Ni^{2+} with the support after impregnation and controlled the redistribution of metal-ion species during drying. Moreover, when redistribution of Ni^{2+} occurred during drying, its transport toward the outer rim of the extrudates came about together with changes of the local en:Ni^{2+} ratio.

1. Introduction

Heterogeneous catalyst bodies are of great importance in many industrial applications. Besides optimal activity, selectivity, and stability, commercial catalyst systems require other characteristics, such as mechanical strength, attrition resistance, and thermal stability. Usually, for industrial applications, preshaped catalyst bodies, with sizes in the range of a few millimeters, are required to diminish the pressure drop inside a fixed-bed chemical reactor.[1−4] A common way of preparing these materials is via pore volume impregnation, in which the support is contacted with an amount of impregnation solution equal to the pore volume. The impregnation step is followed by drying and thermal treatment. During drying and calcination the precursor of the active phase can be redistributed.[5,6] The four major types of macrodistributions in a catalyst body are: uniform, egg-shell, egg-yolk, and egg-white. The formation of the type of macrodistribution is governed by different physicochemical processes taking place during the elementary steps of catalyst preparation and may result in different catalytic properties.[5]

Adsorption/desorption phenomena of the precursor species on the support surface occur during impregnation and drying. In the impregnation step, it depends on different physicochemical properties, such as the surface charge of the support, the charge of the precursor complexes, and the pH and ionic strength of the impregnation solution.[7−9] In the drying process, redistribution of the active phase depends on the drying rate and other properties, such as permeability and viscosity of the impregnation solution.[10−12] To understand the influence of all these parameters on the molecular structure and macrodistribution of the active phase in catalyst bodies during preparation, the use of spectroscopic and diffraction techniques with spatial and time resolution have been recently developed. Raman microscopy,[13] UV−vis microspectroscopy,[14] magnetic resonance imaging (MRI)[15] and X-ray tomography[16] have been applied in the study of Co−Mo hydrotreating catalysts, while UV−vis microspectroscopy has also been used to study the preparation of Co Fischer−Tropsch catalysts.[14b]

Nickel catalysts are commonly used in hydrogenation and hydrogenolysis reactions.[1] These catalysts are usually prepared using a nickel nitrate salt, followed by drying and thermal treatment. An important problem encountered during the preparation of these catalyst systems is the sintering and redistribution that bring about poor dispersion.[6] Another problem might be formation of nickel aluminates and, thereby, poor reducibility.[17] A way of avoiding the migration of Ni^{2+} ions into the bulk structure of alumina might be the addition of complexing agents to the impregnation solution and, consequently, the modification of the molecular structure of the precursor complexes and their interactions with the support. Several studies on the impregnation of different metal-ion precursor solutions containing chelating ligands, such as ethylenediamine (en),[18,19] acetylacetonate (acac),[20,21] ethylenediaminetetracetic acid (edta),[22,23] and citric acid (ca),[12,15c] have indicated that these ligands influence the final metal oxide species and, therefore, their reducibility. Moreover, these ligands are also known to increase the dispersion of the active phase.[19,21,24] In particular, the effect of en on Ni catalysts

* To whom correspondence should be addressed. E-mail: b.m.weckhuysen@uu.nl.

10.1021/jp710676v CCC: $40.75 © 2008 American Chemical Society
Published on Web 04/11/2008

TABLE 1: Overview of the Ni^{2+} Solutions under Study Together with the Characteristic UV−Vis Absorption Bands

	composition			Ni speciation (%)				UV-vis absorption bands		
solutions	Ni/M	En/M	pH	$Ni(H_2O)_6^{2+}$	$Ni(en)(H_2O)_4^{2+}$	$Ni(en)_2(H_2O)_2^{2+}$	$Ni(en)_3^{2+}$	λ_1, nm	λ_2, nm	λ_3, nm
EnNi0	0.5	0	4.7	100	0	0	0	391	654	>1100
EnNi1	0.5	0.5	6.5	17	65	17	1	368	615	961
EnNi2	0.5	1	7.5	0	9	82	9	352	565	924
EnNi3	0.5	1.5	8.5	0	0	3	97	343	546	893
EnNi3pH4	0.5	1.5	4.0	86	14	0	0	391	654	>1100

have been studied in detail by Che et al. using support powders.[18,19,25−28] However, very few studies have been done on the effect of chelating ligands in the preparation of catalyst bodies.[15c,29]

In this paper, the influence of the number of en ligands on the macrodistribution and molecular speciation of Ni^{2+} in γ-Al_2O_3 catalyst bodies during impregnation and drying has been investigated. For this purpose, the transport of different $[Ni(en)_x(H_2O)_{6-2x}]^{2+}$ precursor complexes (with $x = 0-3$) toward the core of the catalyst bodies and their interactions with the alumina support surface, after impregnation, have been monitored with UV−vis microspectroscopy, while the macrodistribution of en was studied after drying with IR microspectroscopy. On the basis of these data, the origin of different macrodistributions will be discussed.

2. Experimental Section

2.1. Catalyst Preparation. $[Ni(en)_x(H_2O)_{6-2x}]^{2+}$ impregnation solutions were prepared at room temperature by adding ethylenediamine (en) (99%, Acros) to an aqueous solution of $Ni(NO_3)_2 \cdot 6H_2O$ (Acros, p.a.) to obtain a final Ni^{2+} concentration of 0.5 M and en:Ni^{2+} molar ratios = 0, 1, 2, and 3. The name and natural pH of the solutions together with the Ni^{2+}-speciation in the precursor solutions are listed in Table 1. EnNi0 corresponds to an aqueous 0.5 M $Ni(NO_3)_2$ solution. One additional solution with an en:Ni^{2+} ratio of 3 was prepared with a final pH of 4 by addition of HNO_3 (p.a., Acros).

Cylindrical γ-Al_2O_3 catalyst bodies (Engelhard, 3 mm in height and diameter) were used. The support had a pore volume of 1.0 mL/g and a surface area of 200 m^2/g. The point of zero charge (pzc) was determined to be 8 by mass titration.[30] The γ-Al_2O_3 pellets were calcined at 450 °C for 8 h and stored at 120 °C until used. In one experiment, HCl-treated alumina pellets, labeled as Al_2O_3-AF, were used as support. These pellets were prepared by passing a flow of HCl(g)/He (10%, 10 mL/min) at 50 °C through a batch of 0.6 g of Al_2O_3 pellets during 5 h.

The supported catalyst materials were prepared by pore volume impregnation on γ-Al_2O_3 (or Al_2O_3-AF) pellets with 0.5 M Ni^{2+} solutions (3 wt % Ni). The Ni^{2+}-solutions were added drop by drop to the support, and the amount added was equal the pore volume plus 10%. After addition of the impregnation solution, manual shaking was applied during 2 min to obtain an even distribution of the solution on the pellets, and the extra solution added (10% of the pore volume) was removed with a pipet. After impregnation, the pellets were kept in a closed vessel for 2 h and dried in a preheated oven under static air at 100 °C for 8 h.

To study the influence of the drying temperature on the macrodistribution and molecular structure of the Ni^{2+} complexes along the catalyst body, three batches of pellets were impregnated with EnNi3 solution and dried at 20, 60, and 90 °C.

2.2. Catalyst Characterization. UV−vis spectra of the impregnation solutions were recorded using a Cary 50 UV−vis spectrophotometer in the range of 240 to 1100 nm. The catalyst materials were measured after impregnation and drying with UV−vis microspectroscopy, making use of an experimental setup previously described in literature.[14a] All measurements on the catalyst bodies were performed applying a line scan on the resulting surface of bisected pellets. The pellets were bisected by inserting them inside a silicon tube; the system tube-pellet was cut with a scalpel. Nine spectra were collected along the cross-section of the bisected pellets with a spatial resolution of around 200 μm, for which 5 min were required. IR spectra on dried pellets were recorded with a Perkin-Elmer Autoimage IR microscope (reflectance mode) with a spatial resolution of 200 μm (200 scans averaging). Energy dispersive analysis of X-rays (EDX) were performed with an XL30SFEG (FEI, The Netherlands) scanning electron microscope. Analysis of the spectra was done with EDAX software (Tilburg, The Netherlands).

Diffuse reflectance near-infrared (NIR) spectra were recorded at room temperature on crushed pellets in the range of 1350−1600 nm using a Varian Cary 500 spectrometer equipped with an integration sphere; a halon was the reference.

3. Results and Discussion

3.1. Chemistry of $[Ni(en)_x(H_2O)_{6-2x}]^{2+}$ Solutions. Table 1 summarizes the species present in the impregnation solutions under study, calculated based on the formation constants of $[Ni(en)_x(H_2O)_{6-2x}]^{2+}$ ($x = 1-3$) complexes, as a function of the pH of the solutions.[31]

Experimental UV−vis absorption bands of the solutions are also listed in Table 1. Three bands were observed in all solutions at around 350, 600, and 1000 nm. Assuming an octahedral symmetry of the Ni^{2+} complexes, these bands can be assigned to the $^3T_{1g}(P) \leftarrow {}^3A_{2g}$, $^3T_{1g}(F) \leftarrow {}^3A_{2g}$ and $^3T_{2g} \leftarrow {}^3A_{2g}$ d−d spin-allowed transitions, repectively.[32] A blue shift of the Ni^{2+} d−d transition bands was observed as en:Ni^{2+} ratio increased from 0 to 3, indicating that en ligands, which are stronger ligands in the spectrochemical series than water, entered into the first coordination sphere of Ni^{2+}.[32] Ni^{2+} d−d bands were responsible of the characteristic colors that these solutions had, from green for solution EnNi0 passing through blue (solution EnNi1) to different shades of purple (solutions EnNi2 and EnNi3). A band at around 300 nm was observed in all impregnation solutions, which corresponded to a NO_3^- $n \rightarrow \pi^*$ charge-transfer transition.[32] Solution EnNi0 showed, in addition, a band at around 730 nm, which can be assigned to a d−d spin-forbidden band of Ni^{2+}.[32]

The UV−vis spectrum of solution EnNi3pH4 resembled that of solution EnNi0 because of its acidification. Protonation of en ligands occurred causing the formation of complex $[Ni(H_2O)_6]^{2+}$ (86%), as reported in Table 1.

3.2. γ-Al_2O_3 Surface. Figure 1a shows the diffuse reflectance NIR spectrum on crushed γ-Al_2O_3 in the region between 1350 and 1600 nm. This region, characteristic for the first overtone OH stretching vibrations (2ν), shows a broad band with three maxima at 1384, 1416, and 1446 nm. The maxima indicated the presence of surface OH groups with different basicity: basic OH groups are characteristic of the signal at 1384 nm, neutral

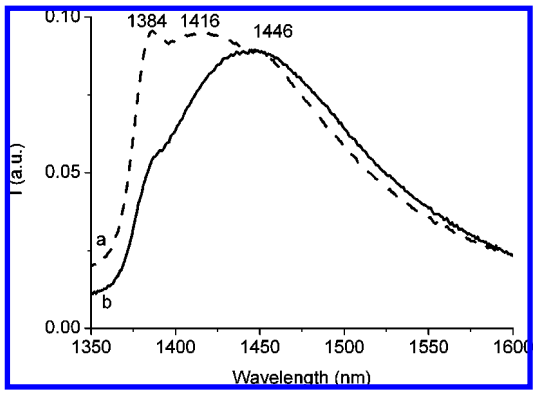

Figure 1. NIR spectra measured on crushed Al_2O_3 (a) and on chlorinated alumina, Al_2O_3-AF (b).

groups at 1416 nm, and acidic groups at 1446 nm.[33,34] These basic, neutral, and acidic surface OH groups will be referred as Al_B-OH, Al_n-OH, and Al_A-OH, respectively. The acid−base properties of alumina surface hydroxyl groups are determined by the coordination of the OH group to Al^{3+} as follows: different coordination to Al^{3+} gives rise to a different net charge on the oxygen: the higher the negative charge on the oxygen, the more basic the hydroxyl groups.[8,35] It has to be considered, however, that there are more than three different hydroxyl groups on the alumina surface.[35]

Because of the different acid−base properties of alumina surface hydroxyl groups, these ionize in the presence of aqueous solutions and can become protonated in an acidic medium ($pH_{solution}$ < pzc), leading to a bulk pH increase of the solution and a positively charged alumina surface, or deprotonated in a basic medium ($pH_{solution}$ > pzc).[36] Basic OH (Al_B-OH) groups will become more easily protonated in an acidic medium whereas Al_A-OH will deprotonate in a basic medium, see eq 1 and 2:

$$Al_B\text{-}OH + H^+ \leftrightarrow Al_B\text{-}OH_2^+ \quad (1)$$

$$Al_A\text{-}OH + OH^- \leftrightarrow Al_A\text{-}O^- + H_2O \quad (2)$$

The NIR spectrum of HCl-treated alumina, Al_2O_3-AF (Figure 1b), showed a broad band centered at 1446 nm and a shoulder at 1384 nm. The lower intensity of the reflection at 1384 nm compared to nontreated alumina (Figure 1a) was consistent with the consumption of basic hydroxyl groups due to the chlorination treatment, according to the following reaction:[37]

$$Al_B\text{-}OH + HCl \leftrightarrow Al_B\text{-}Cl + H_2O \quad (3)$$

Moreover, the shift of the band maximum to longer wavelengths indicated acidification of alumina, as it is known to occur.[38,39]

3.3. Impregnation Step. *UV−vis Microspectroscopy after Initial Contact Solution-Support.* The impregnation process was monitored by means of UV−vis microspectroscopy. Spectra collected from the edge to the center of pellets, 5 min after impregnation, with solutions EnNi0 to EnNi3 are shown in Figure 2. Ni^{2+} was detected with a rather uniform absorption profile of the d−d bands in the four samples, and a fast migration rate of Ni^{2+} complexes was apparent.

Impregnated EnNi0 pellets showed a uniform distribution of $[Ni(H_2O)_6]^{2+}$ complexes with bands λ_1 and λ_2 at 400 and 660 nm (Figure 2a). Ni^{2+} d−d bands showed a constant intensity along the cross-section of the pellet, indicating a fast transport of Ni^{2+} toward the core of the pellets. Thus, weak interactions

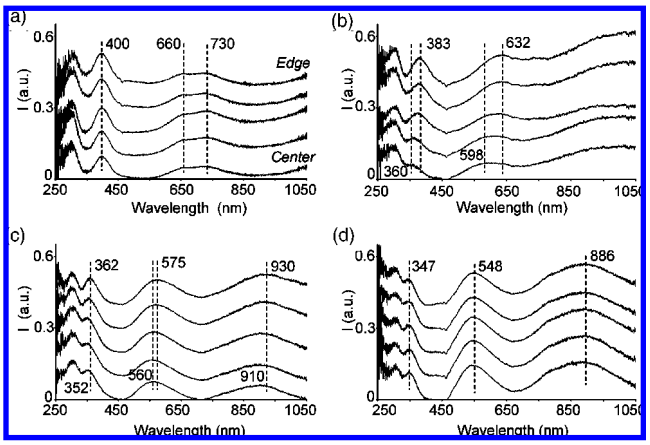

Figure 2. UV−vis spectra collected from the edge to the center of bisected pellets, 5 min after impregnation: (a) EnNi0, (b) EnNi1, (c) EnNi2, and (d) EnNi3.

or noninteractions between $[Ni(H_2O)_6]^{2+}$ and alumina surface were taking place. These bands appeared slightly shifted to longer wavelengths compared to the bands for the EnNi0 solution, see Table 1. The charge-transfer band of NO_3^- at 300 nm and the Ni^{2+} d−d spin-forbidden transition at around 730 nm were also observed. Band λ_3, of which maximum absorption in solution appeared at wavelengths longer than 1100 nm, was beyond the detection limits of the setup.

The red shift of the Ni^{2+} d−d bands could be explained as follows. The low pH of an aqueous solution of nickel nitrate is brought about by the following equilibrium:[36]

$$[Ni(H_2O)_6]^{2+} + H_2O \leftrightarrow [Ni(H_2O)_5(OH)]^+ + H_3O^+ \quad (4)$$

When an $[Ni(H_2O)_6]^{2+}$ solution contacts the alumina support, the formation of $[Ni(H_2O)_5(OH)]^+$ is enhanced, as the alumina basic hydroxyl groups will consume protons (eq 1). The d−d absorption bands of this species appear at slightly longer wavelengths compared to that of $[Ni(H_2O)_6]^{2+}$ since OH^- is a weaker ligand, in the spectrochemical series, than H_2O.[32]

When γ-Al_2O_3 pellets were impregnated with solutions EnNi1 and EnNi2, a shift of the d−d absorption bands, λ_1, λ_2, and λ_3, to shorter wavelengths was monitored from the edge to the center of the pellets (Figures 2b and 2c). In EnNi1 sample, Ni^{2+} d−d bands λ_1 and λ_2 at the edges were measured at 383 and 632 nm, respectively; i.e., λ_1 and λ_2 shifted to longer wavelengths compared to the corresponding bands in the precursor EnNi1 solution (Table 1). Additionally, in the center of the extrudates, λ_1 and λ_2 bands appeared at 360 and 598 nm with band λ_2 being very broad. The maximum absorption position of band λ_3 was difficult to determine because of the broadness of the band and the intrinsic detection limits of the setup. Visual inspection revealed the interior of the pellet to turn from blue, close to the edges, to purple, close to the core, in correspondence with the blue-shift of the d−d bands toward the core of the pellets.

These observations can be explained by realizing that when the complex $[Ni(en)(H_2O)_4]^{2+}$ contacted the alumina support (the edges), the acidic OH groups of alumina may partly protonate en ligands of $[Ni(en)(H_2O)_4]^{2+}$ complexes, forming enH^+ and enH_2^{2+}, the former not indicated for simplicity:

$$[Ni(en)(H_2O)_4]^{2+} + 2\ Al_A\text{-}OH + 2\ H_2O \leftrightarrow [Ni(H_2O)_6]^{2+} + 2\ Al_A\text{-}O^- + enH_2^{2+} \quad (5)$$

When these species were transported toward the core of the pellet, enH_2^{2+} could deprotonate because of its interaction with Al_B-OH, losing either one (enH^+) or even both protons (en); therefore, increasing the pH of the solution toward the core of the pellets, and deprotonated en could react further with the precursor complex to form $[Ni(en)_x(H_2O)_{(4-2x)}]^{2+}$, $x > 1$, (eq 6 and 7):

$$enH_2^{2+} + 2\ Al_B\text{-}OH \leftrightarrow en + 2\ Al_B\text{-}OH_2^{+} \quad (6)$$

$$[Ni(en)(H_2O)_4]^{2+} + x\ en \leftrightarrow [Ni(en)_{1+x}(H_2O)_{(4-2x)}]^{2+} + 2x\ H_2O \quad (7)$$

The gradient of Ni^{2+} species 5 min after impregnation could only develop because after this time there was still not an even distribution of Ni^{2+} concentration inside the pellets and enH_2^{2+}/en moved faster than $[Ni(en)(H_2O)_4]^{2+}$. In the center of the pellets the concentration of Ni^{2+} was lower than the concentration of surface hydroxyl groups, making it possible to locally and temporarily create Ni^{2+} complexes which are only stable at high pH.

Pellets impregnated with EnNi2 solution (Figure 2c) showed a red shift of Ni^{2+} d−d bands in the edges (362, 575, and 930 nm) compared to the precursor solution (Table 1) whereas in the core of the extrudates, the bands were measured at the same positions as in the solution (352, 560, and 910 nm), indicating the presence of $[Ni(en)_2(H_2O)_2]^{2+}$ species. A similar scheme of reactions is proposed to occur in the edges of EnNi2 impregnated pellets as for EnNi1, see eqs 8 and 9. Again, enH_2^{2+} can partially or totally deprotonate forming enH^+ or en. Equation 9 only shows the total deprotonation of enH_2^{2+} for simplicity.

$$[Ni(en)_2(H_2O)_2]^{2+} + 2x\ Al_A\text{-}OH + 2x\ H_2O \leftrightarrow [Ni(en)_{2-x}(H_2O)_{2+2x}]^{2+} + x\ enH_2^{2+} + 2x\ Al_A\text{-}O^{-} \quad (8)$$

$$enH_2^{2+} + 2\ Al_B\text{-}OH \leftrightarrow en + 2\ Al_B\text{-}OH_2^{2+} \quad (9)$$

In the core of the pellet, $[Ni(en)_2(H_2O)_2]^{2+}$ was regenerated.

Figure 2d shows the UV−vis profile measured from the edge to the center on an impregnated pellet with solution EnNi3. Ni^{2+} d−d bands appeared uniformly distributed at 347, 548, and 886 nm, the same positions as in the impregnation solution (Table 1) indicating that the $[Ni(en)_3]^{2+}$ complex did not interact strongly with the support.

The fast penetration rate of $[Ni(en)_3]^{2+}$ complex together with the stability of its molecular structure can be explained with the "physical adsorption" model developed by Regalbuto et al.[7] which proves that, for some systems, adsorption of metal complexes during impregnation occur primarily by electrostatic interactions. The pH of the solution was very close to the pzc of the support, so the support had an overall zero surface charge. No interactions between Ni^{2+} complexes and alumina took place, and the concentration of en molecules was high enough to avoid their protonation. Therefore, the pH of the solution inside the pores did not change.

UV−vis Microspectroscopy after Equilibration. After 2 h of equilibration, uniform distributions of Ni^{2+} complexes were measured in all the impregnated samples, as shown in Figure 3.

The 2-h impregnated EnNi0 sample showed a uniform distribution of octahedral Ni^{2+} complexes with d−d transition bands λ_1 and λ_2 at 400 and 662 nm; λ_3 was beyond the detection range of the setup (Figure 3a). The spectra collected along the cross-section of the pellet were identical of that 5 min after impregnation (Figure 2a). One possible reason to justify the position of bands λ_1 and λ_2 could be that specific interactions between $[Ni(H_2O)_6]^{2+}$ and hydroxyl groups of alumina took place a certain time after impregnation (up to 2 h), eqs 10 and 11:

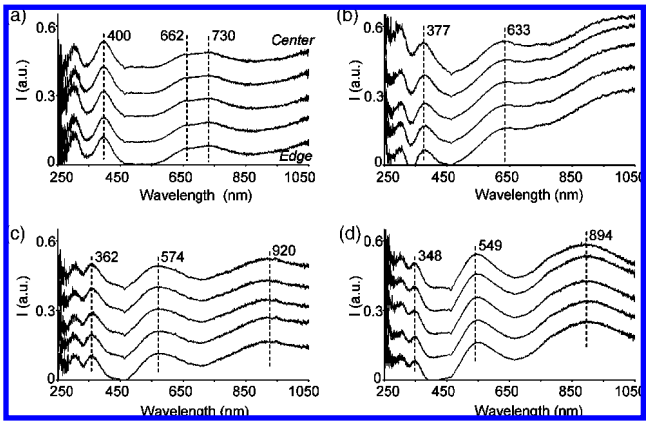

Figure 3. UV−vis spectra measured after 2 h of equilibration on bisected pellets from the edge to the core: (a) EnNi0, (b) EnNi1, (c) EnNi2, and (d) EnNi3.

$$Al{-}OH + [Ni(H_2O)_6]^{2+} \leftrightarrow [Al{-}O{-}Ni(H_2O)_5]^{+} + H_3O^{+} \quad (10)$$

$$2\ Al{-}OH + [Ni(H_2O)_6]^{2+} \leftrightarrow [(Al{-}O)_2Ni(H_2O)_4] + 2\ H_3O^{+} \quad (11)$$

However, it should also be considered that, during this time, it was possible that no specific interactions with the support took place, and the bands were shifted because of the presence of partially hydrolyzed $[Ni(H_2O)_{6-x}(OH)_x]^{2-x}$ complex formed by the influence of the alumina hydroxyl surface, as mentioned to occur immediately after impregnation.

Along the cross-section of impregnated EnNi1 pellets after 2 h of equilibration, two d−d bands with the maximum absorption at 377, 633 nm were measured with constant absorption intensity (Figure 3b). Again, the maximum absorption of band λ_3 was difficult to determine. The gradient of species $[Ni(en)_x(H_2O)_{6-2x}]^{2+}$ created after initial contact of the solution with the support had disappeared after 30−60 min of impregnation. The spectra collected in all the positions, after 2 h of equilibration, were very similar to that of $[Ni(en)(H_2O)_4]^{2+}$ in solution, but the red shift of Ni^{2+} d−d bands indicated that weaker ligands (in the spectrochemical series) entered Ni^{2+} first coordination sphere. Grafting to the alumina surface could be a possible mechanism to explain the band shifts observed, where alumina hydroxyl groups act as nucleophiles as follows:

$$[Ni(en)(H_2O)_4]^{2+} + Al{-}OH \leftrightarrow [Al{-}O{-}Ni(en)(H_2O)_3]^{+} + H_3O^{+} \quad (12)$$

$$[Ni(en)(H_2O)_4]^{2+} + 2\ Al{-}OH \leftrightarrow [(Al{-}O)_2Ni(en)(H_2O)_2] + 2\ H_3O^{+} \quad (13)$$

EnNi2 pellets, after 2 h of equilibration, showed Ni^{2+} d−d bands at 362, 574, and 920 nm evenly distributed along the cross-section of the pellet (Figure 3c). These bands were shifted to longer wavelengths compared to EnNi2 solution, Table 1. In the core of the pellets, bands appeared also red-shifted compared

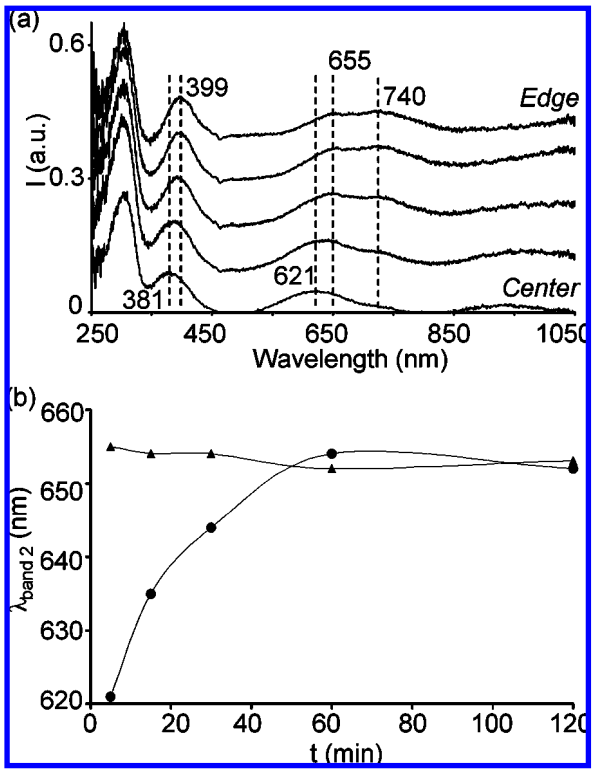

Figure 4. (a) UV−vis profile measured on EnNi3pH4 bisected pellet, from the edge to the core, 5 min after impregnation. (b) Position of band λ_2 at the edge (▲) and in the core (●) as a function of the time after impregnation on pellet EnNi3pH4.

to the UV−vis spectra measured at that position 5 min after impregnation (Figure 2c). As in EnNi1 sample, a change in Ni^{2+} coordination sphere occurred with time after impregnation, where possibly water ligands were partially substituted by surface hydroxyl groups from the alumina:

$$[Ni(en)_2(H_2O)_2]^{2+} + Al{-}OH \leftrightarrow [Al{-}O{-}Ni(en)_2(H_2O)]^{+} + H_3O^{+} \quad (14)$$

$$[Ni(en)_2(H_2O)_2]^{2+} + 2\ Al{-}OH \leftrightarrow [(Al{-}O)_2Ni(en)_2] + 2\ H_3O^{+} \quad (15)$$

The UV−vis profile measured on EnNi3 impregnated pellets, after 2 h, shown in Figure 3d, was the same as after 5 min of impregnation (Figure 2d). Ni^{2+} d−d bands were measured at 348, 549, and 894 nm, indicating that $[Ni(en)_3]^{2+}$ species were present uniformly distributed inside the pellets without interacting with the alumina hydroxyl surface.

Che et al. proposed a spectrochemical series of surface ligands from supports in which $Al{-}O^{-}$ is a weaker ligand than H_2O.[40] Moreover, the grafting that $[Ni(en)_x(H_2O)_{6-2x}]^{2+}$ ($x = 1, 2$) undergo on a powder support has been also studied by means of spectroscopic techniques which demonstrated the formation of Al−O−Ni bonds after the different catalyst preparation steps.[18,19] The specific adsorption of $[Ni(H_2O)_6]^{2+}$on γ-Al_2O_3 during the wet step of catalyst preparation was already reported by Geus et al.; they proposed a similar mechanism of Ni^{2+} interaction with the hydroxyl surface of alumina.[41] Furthermore, several studies performed by Lycourgiothis et al. demonstrated the formation of inner-sphere Co surface complexes during the wet step of cobalt-on-alumina catalyst preparation, which would be parallel to the inner sphere Ni^{2+} complexes formed on alumina surface.[42] It is still under debate which are the OH

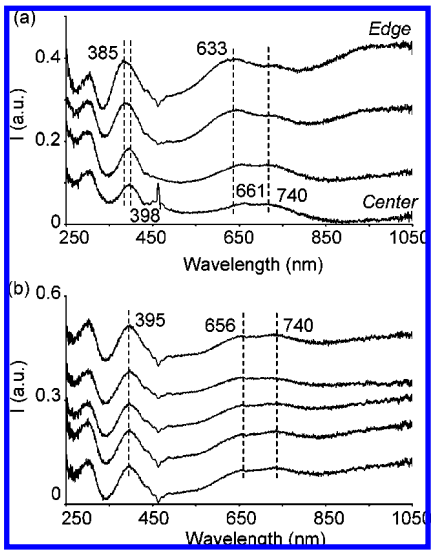

Figure 5. UV−vis spectra measured 5 min after impregnation (a) and 2 h after equilibration (b) of EnNi1 solution on Al_2O_3-AF pellets.

groups involved in these interactions. It has to be taken into account that, after impregnation, only a very small amount of basic hydroxyl groups would become protonated, since the concentration of H^+ coming from the solution inside alumina pores is very low, and can be negligible. Therefore, the interactions between the support's surface and $[Ni(en)_x(H_2O)_{6-2x}]^{2+}$ occurs through the neutral form of basic or acidic OH groups. Most likely, it occurs through the neutral form of basic OH groups, since these are the most nucleophile.[35]

UV−vis Microspectroscopy on Acidified EnNi3. The UV−vis profile measured from the edge to the center of EnNi3pH4 pellet 5 min after impregnation is shown in Figure 4a. The spectra changed drastically from the edge to the core. The typical UV−vis spectrum of $[Ni(H_2O)_6]^{2+}$ complex was observed in the edges of the pellets, whereas, in the core, a marked shift of the bands to shorter wavelengths was observed, with d−d bands λ_1 and λ_2 at 381 and 621 nm. The spectrum in the core of the pellets was close to that of $[Ni(en)(H_2O)_4]^{2+}$. The band shifting came along with a change of color inside the extrudates from green, in the outer area, to purple, in the center. The blue shift of the absorption bands toward the core of the pellets indicated a pH increase of the solution in that direction and, therefore, a change in Ni^{2+} coordination sphere. Toward the core, enH_2^{2+} became partially (enH^+) or totally deprotonated (en) because of its interaction with the basic Al_B-OH groups. The deprotonated species en could then interact with Ni^{2+} to form $[Ni(en)_x(H_2O)_{6-2x}]^{2+}$ (eq 6 and 16).

$$[Ni(H_2O)_6]^{2+} + x\ en \leftrightarrow [Ni(en)_x(H_2O)_{6-2x}]^{2+} + 2x\ H_2O \quad (16)$$

Figure 4b represents the position of band λ_2 measured in the edge and in the center of impregnated EnNi3pH4 pellet at certain times after impregnation. After approximately 60 min of equilibration, bands λ_1 and λ_2 were measured at the same positions (397 and 654 nm) in the edges and in the core of the pellet, indicating the presence of $[Ni(H_2O)_6]^{2+}$, without interacting substantially with the support.

The impregnation process of sample EnNi3pH4 on γ-Al_2O_3 pellets followed the same trend observed in samples EnNi1 and EnNi2 (Figures 2a, 2b and 3a, 3b). Most likely, the impregnation of $[Ni(en)_x(H_2O)_{6-2x}]^{2+}$ ($x = 1, 2$) on γ-Al_2O_3 pellets occurs in two steps:

(1) Imbibition: Ni^{2+} complexes move fast toward the core of the pellets because of capillary forces. It was measured that the Ni^{2+} molecular structure changed strongly during its transport toward the core because of the effect that both Al_B-OH and Al_A-OH have on the formation/cleavage of $[Ni(en)_x(H_2O)_{6-2x}]^{2+}$. However, grafting is not taking place since Ni^{2+} transport toward the core is very fast.

(2) Equilibration: After 30−60 min, Ni^{2+} was uniformly distributed in the pellets with a different Ni^{2+} first coordination sphere compared to that of the solution. One possibility would be that labile H_2O ligands in $[Ni(en)(H_2O)_4]^{2+}$ or $[Ni(en)_2(H_2O)_4]^{2+}$ had been exchanged by one or two hydroxyl groups from alumina surface.

UV−vis Microspectroscopy on Chlorinated Alumina Pellets. Figure 5 shows the UV−vis profile from the edge to the center of an Al_2O_3-AF pellet impregnated with solution EnNi1 5 min after impregnation and 2 h of equilibration. Five minutes after impregnation (Figure 5a), Ni^{2+} was already present in the center of the pellet. The intensity of the absorption bands was lower in the core than in the edges, which was also visually observed, and Ni^{2+} transport was slower than on nontreated alumina pellets. A change in the molecular structure of Ni^{2+} along the cross-section of the pellet was also measured. In the edge, Ni^{2+}d−d bands λ_1 and λ_2 were measured at 385 and 633 nm. Band λ_3 was centered above 1100 nm with a shoulder at around 950 nm. This spectrum indicated the presence of mainly $[Ni(en)(H_2O)_4]^{2+}$ complexes, as if EnNi1 solution was impregnated on nontreated alumina (Figure 2b). In the center, the spectrum resembled that of $[Ni(H_2O)_6]^{2+}$ with bands λ_1 and λ_2 centered at 398 and 665 nm and the very characteristic spin-forbidden band at around 730 nm with a similar intensity as λ_2. Band λ_3 was beyond the energy detection range.

The change in Ni^{2+} molecular structure was due to a decrease in the pH of the solution toward the core of the pellets caused by the fact that Al_2O_3-AF was an acidic support and the concentration of basic hydroxyl sites (Al_B-OH) was negligible (Figure 1). Toward the core, $[Ni(en)(H_2O)_4]^{2+}$ fell apart because of protonation of en molecules by Al_A-OH groups to form enH^+ and enH_2^{2+}, as shown in eq 5. Since no Al_B-OH was present on the alumina surface, deprotonated en molecules could not be formed and the precursor complex could not be regenerated.

The slow transport of Ni^{2+} observed toward the core, compared to its dynamics on nontreated alumina, was caused by the negative alumina surface charge compared to nontreated alumina. After 2 h of equilibration (Figure 5b), Ni^{2+} was measured along the cross-section of Al_2O_3-AF pellets with a uniform concentration of $[Ni(H_2O)_6]^{2+}$ species (bands λ_1 and λ_2 at 395 and 656 nm). Clearly, $[Ni(H_2O)_6]^{2+}$ remained as the stable species throughout the support body.

3.4. Drying Step. *UV−vis Microspectroscopy after Drying.* Figure 6 shows the UV−vis spectra collected on pellets EnNi0−EnNi3 after drying at 100 °C for 8 h. Different species were detected along the cross-section of alumina pellets as a function of the ratio en:Ni^{2+}. EnNi0 and EnNi1 dried pellets showed a uniform distribution of a single Ni^{2+}complex (Figures 6a and 6b), whereas EnNi2 and EnNi3 dried pellets presented a gradient of $[Ni(en)_x(H_2O)_{6-2x}]^{2+}$ species with the core of the pellets showing Ni-en species poorer in en than the edges (Figures 6c and 6d).

Dried pellets EnNi0 showed three bands at 404, 670, and 750 nm; the latter corresponds to a Ni^{2+} d−d spin-forbidden band (Figure 6a). These bands, shifted to longer wavelengths compared to the solution and to the impregnated pellets, indicated an octahedral symmetry of Ni^{2+} in a uniform distribution inside the pellets, and H_2O ligands most probably exchanged

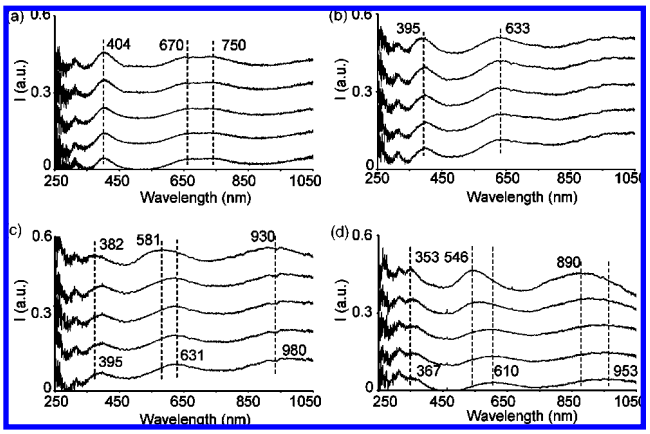

Figure 6. UV−vis spectra from the edge to the center of bisected pellets after drying: (a) EnNi0, (b) EnNi1, (c) EnNi2, and (d) EnNi3.

by surface hydroxyl groups. EnNi1 dried pellets showed Ni^{2+} d−d bands λ_1 and λ_2 at the same positions as 2 h after impregnation (Figure 6b). These bands might be due to the inner-sphere complexes $[(Al-O)_2Ni(en)(H_2O)_2]$ or $[Al-O-Ni(en)(H_2O)_3]^+$ that might form during the impregnation step. In both samples, band λ_3 was beyond the energy detection limit of the setup.

EnNi2 and EnNi3 dried pellets showed a gradual red-shift of the Ni^{2+} d−d bands from the edge to the center of the pellets (Figure 6c and 6d). Ni^{2+} d−d bands λ_1, λ_2, and λ_3 of EnNi2 dried pellets were measured at 382, 581, and 930 nm close to the edge, and at 395, 631, and 980 nm in the core of the pellets, respectively (Figure 6c). Drying induced Ni^{2+} speciation, and the core of the extrudates contained Ni^{2+} complexed to less than two en molecules, as deduced from the position of Ni^{2+} d−d bands. The spectrum at this position was identical to that measured on the center of EnNi1 dried sample; i.e., Ni^{2+} contained in its coordination sphere one molecule of en and one or two oxygens from alumina hydroxyl groups. Moreover, the intensity of the absorption bands was very similar along the cross-section of the pellets. It is difficult to say whether Ni^{2+} followed the same trend as en molecules or it was uniformly distributed inside the pellets.

On dried EnNi3 sample (Figure 6d), Ni^{2+} d−d bands λ_1, λ_2, and λ_3 were measured at 353, 546, and 890 nm in the edges (indicative of $[Ni(en)_3]^{2+}$ complex) and at 367, 610, and 953 nm in the core of the pellets. The core of the extrudates contained Ni^{2+} species complexed to less than three en molecules, where en was exchanged with hydroxyl groups of alumina. An important decrease in the intensity of the Ni^{2+} d−d transitions bands was observed going from edge to core. Because of the different absorption coefficients of $[Ni(en)_x(H_2O)_{6-2x}]^{2+}$ it was difficult to quantitatively link the difference in intensity to a difference in Ni^{2+} concentration.

Figure 7 shows the 1D line-scans of Ni wt % with the position inside the pellets EnNi1− EnNi3 measured with SEM-EDX. This measurement was not performed in EnNi0 dried pellets because the UV−vis profile (Figure 6a) already shows the uniform profile of Ni^{2+}. In the three line-scans, the points obtained were rather scattered because of the roughness of the cross-sections. The overall Ni^{2+} content measured was around the intake of 3 wt %. A rather uniform Ni concentration was measured on EnNi1 dried pellets (Figure 7a). In samples EnNi2 and EnNi3 (Figure 7b and 7c), Ni^{2+} content was above 3 wt % at the edges and in the center was below this value. There was a tendency toward Ni^{2+} egg-shell distributions with increasing the en:Ni^{2+} ratio.

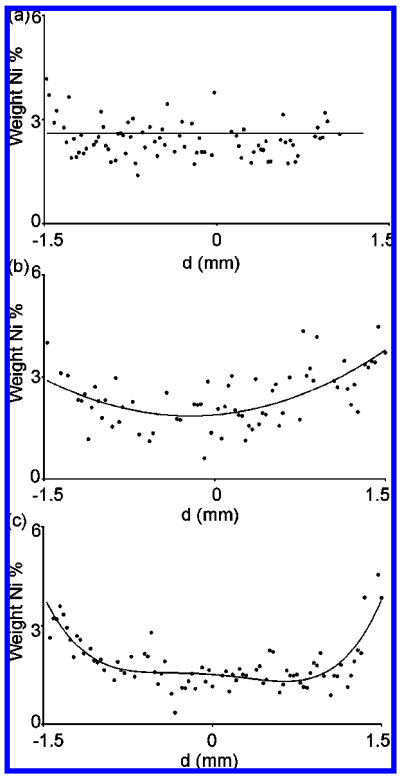

Figure 7. Ni profiles after drying as measured by SEM-EDX: (a) EnNi1, (b) EnNi2, (c) EnNi3.

Combining the UV−vis data after drying (Figure 6) with the Ni^{2+} profiles measured with EDX (Figure 7), we see that the different mobilities of the Ni precursor complexes observed after drying can only be explained by assuming a specific interaction between the alumina surface and the Ni complexes which contained H_2O as part of its first coordination sphere, via grafting (exchange of water ligands with surface OH groups) before drying. During drying, $[Ni(en)_3]^{2+}$ complex is transported together with the solvent, toward the outer surface of the pellets because of the absence of interactions between this complex and alumina in the impregnation step (Figures 3d and 6d). On the other hand, when the impregnation solution contains $[Ni(H_2O)_6]^{2+}$ or $[Ni(en)(H_2O)_4]^{2+}$, the transport of Ni^{2+} toward the outer surface during the drying step is not possible (Figures 3 and 6a,b) because of the stronger interactions between these complexes and the support that started taking place some time after impregnation, as proposed in eqs 10−13.

IR Microspectroscopy on Dried Pellets. The distribution of the chelating ligand, en, was monitored with IR microspectroscopy. Figure 8 shows the IR spectra between 3500 and 2500 cm^{-1} measured from the edge to the core of the EnNi1−EnNi3 dried pellets. In this region, all the samples showed several absorption bands, more or less intense: a doublet at around 2940 and 2890 cm^{-1} typical of C−H stretching vibrations and two bands at around 3330 and 3284 cm^{-1} characteristic of $N-H_2$ stretching vibrations (the latter observed only in sample EnNi3, Figure 8c) from en ligands complexing Ni^{2+} in an octahedral symmetry.[43]

Dried EnNi1 sample (Figure 8a) showed the two bands at 2944 and 2894 cm^{-1} characteristic of C−H stretching vibrations in a rather even distribution along the cross-section of the pellets. These indicated a uniform profile of en groups on the support agreeing with the uniform distribution of $[Ni(en)(H_2O)_{4-x}(Al-O)_x]^{+2-x}$ ($x = 1$ or 2) species proposed from the UV−vis data (Figure 6b).

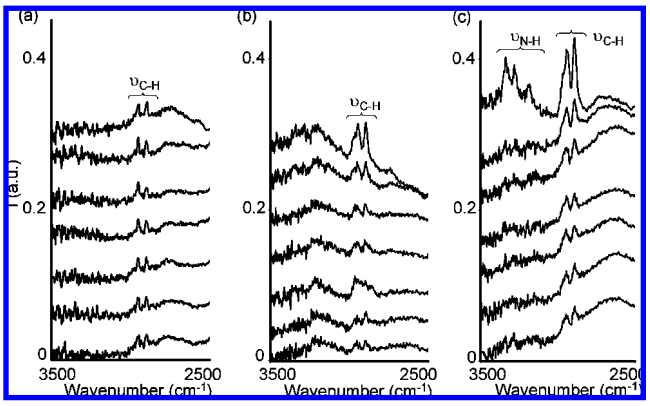

Figure 8. IR spectra collected from the edge to the center of dried bisected pellets in the 3500−2500 cm^{-1} region: (a) EnNi1, (b) EnNi2, and (c) EnNi3.

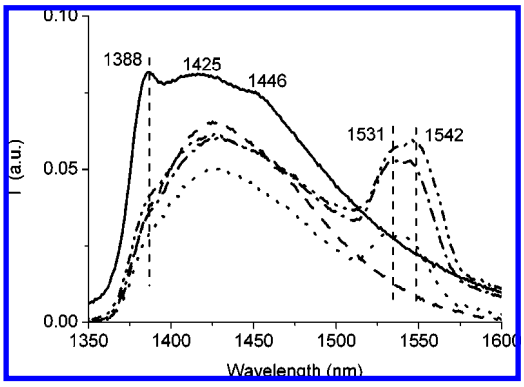

Figure 9. NIR spectra of dried and crushed samples EnNi0 (− −), EnNi1 (····), EnNi2 (− · −) and EnNi3(− ·· −). NIR spectrum of Al_2O_3 is shown as a reference (−).

An egg-shell distribution of en, as deduced from the intensity the C−H stretching vibrations at 2940 and 2892 cm^{-1}, was measured in dried pellets EnNi2 (Figure 8b). The similar intensity of the bands in dried samples EnNi1 and EnNi2 shows that the concentration of en species in the core of the pellets was the same in both samples, in line with what was observed with UV−vis (Figures 6b and 6c). Dried pellets EnNi3 (Figure 8c) also exhibited an egg-shell distribution of en ligands with the C−H stretching vibrations at 2936 and 2892 cm^{-1}, and the N−H stretching vibrations at 3338 and 3282 cm^{-1} more intense in the edges than toward the core of the pellet. The latter bands were not observed in samples EnNi1 and EnNi2 probably because of the lower concentration of en ligands compared to sample EnNi3.

Diffuse Reflectance NIR on Crushed EnNix Pellets. Figure 9 shows the NIR spectra in the region between 1350 and 1600 nm on crushed pellets EnNi0-EnNi3 after drying. The spectra in this region consisted of several bands due to (i) first ν(OH) overtones of basic, neutral, and acidic surface hydroxyl groups at 1388, 1425, and 1446 nm, respectively, and (ii) first ν(NH) overtones of en molecules at around 1531 and 1542 nm.[33,34] These spectra show an increase in intensity of the NH_2 overtone band from en, with increasing ratio en:Ni^{2+}. The combination band ($\nu + \lambda$) of the NH_2 stretching vibration (not shown here for brevity) showed the same trend. Thus, the overall molar ratios from the precursor solutions were kept after drying at 100 °C. Moreover, a consumption of alumina surface hydroxyl groups in all the samples can be observed, with respect to γ-Al_2O_3 surface. This information supports the proposed grafting mechanism of interaction, 2 h after impregnation, between

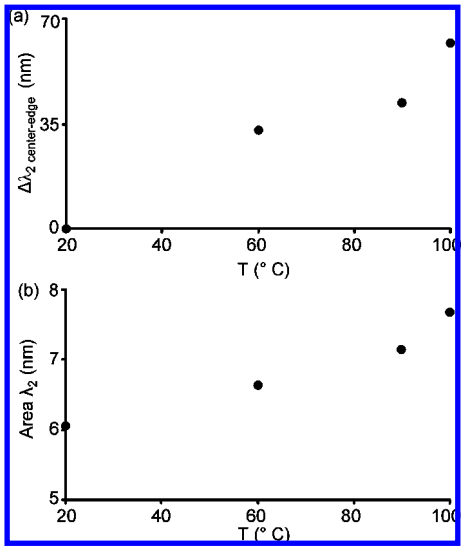

Figure 10. (a) Difference in the position of band λ_2 in EnNi3dried pellets, between the center and the edge, as a function of drying temperature. (b) Area of band λ_2 measured at the edges of impregnated EnNi3 pellets dried at different temperatures.

$[Ni(en)_x(H_2O)_{6-2x}]^{2+}$ ($x = 0-2$) precursor complexes and the alumina hydroxyl surface.

Effect of the Drying Temperature on EnNi3 Sample. The effect of the drying temperature on the UV−vis spectra of EnNi3 pellets was studied, and the results are shown in Figure 10. Figure 10a represents the difference (in wavelengths) between the position of band λ_2 measured in the center and in the edge of a pellet ($\Delta\lambda_2 = \lambda_2^{center}-\lambda_2^{edge}$) as a function of the drying temperature.

Pellets dried at RT showed a uniform purple color along the scanned area with the three Ni^{2+} d−d absorption bands at the same positions as for the impregnated EnNi3 pellets after 2 h, denoting that the complex $[Ni(en)_3]^{2+}$ remained unchanged and uniformly distributed inside the pellet; i.e., the drying step did not have an influence on the nature or distribution of the active component.

When the drying temperature was increased to 60 °C or above, the UV−vis spectra along the cross-section of the dried pellets showed a gradual change of the bands. The spectra measured in the edge of the pellets dried at 60, 90, and 100 °C was very similar to that of the impregnated pellets after 2 h, with the three Ni^{2+} d−d bands characteristic of $[Ni(en)_3]^{2+}$ species. In the center of the pellet, the spectra suffered a red shift of the bands, indicative of the presence of species with lower concentration of en groups bonded to the Ni^{2+} ion. As it is concluded from Figure 10a, the red shift of λ_2 in the center of the pellets increased with the drying temperature; i.e., the higher the drying temperature, the poorer the core in en molecules.

A semiquantitative analysis of the amount of $[Ni(en)_3]^{2+}$ complex at the edges of the pellets as a function of the drying temperature was performed and represented in Figure 10b. In this figure, the area under band λ_2 measured in the edge of the dried pellets is represented versus the drying temperature. The graph shows that the concentration of $[Ni(en)_3]^{2+}$ in the edges increased with the drying temperature; i.e., higher drying temperatures induced a more substantial transport of $[Ni(en)_3]^{2+}$ toward the external surface of the pellets. However, $[Ni(en)_3]^{2+}$ that remained behind fell apart, and en molecules were partially substituted by surface OH groups.

4. Conclusions

The different $[Ni(en)_x(H_2O)_{6-2x}]^{2+}$ ($x = 0-3$) complexes in the precursor solutions together with pH have a strong influence on the first steps of the catalyst preparation process. During the first hour after contacting the impregnation solution with the support, a strong influence of the alumina surface on the molecular structure of Ni^{2+} during its transport toward the core of the pellets was measured. When solutions with a pH below the pzc of Al_2O_3 ($en:Ni^{2+} = 1, 2$) were impregnated, the precursor complexes fell apart inside alumina pores by cleavage of the $Ni-NH_2$ bonds due to the action of acidic Al_A-OH. However, the precursor complexes could be regenerated because of the basic alumina surface OH groups. Moreover, Ni^{2+} moved fast toward the core, indicating that no interactions occurred between Ni^{2+} and the alumina surface. After the first hour of contact between the solution and the support, a grafting mechanism started taking place by which Ni^{2+} specifically adsorbed onto alumina via an exchange reaction between labile water ligands and hydroxyl groups of alumina; most likely, basic OH groups were responsible for this interaction. The strongest adsorption to the surface occurred for the ratio $en:Ni^{2+} = 1$, whereas ratios 0 and 2 showed similar adsorption to the surface. On the other hand, when Ni^{2+} was not surrounded by water ligands, it could not be adsorbed on alumina surface ($en:Ni^{2+} = 3$). When the acidity of the alumina was increased, the $[Ni(en)(H_2O)_4]^{2+}$ precursor complex fell apart when contacting the support because of protonation of en, and it could not be regenerated because of the lack of basic hydroxyl groups.

The adsorption of $[Ni(en)_x(H_2O)_{6-2x}]^{2+}$ onto the alumina surface, before drying, was responsible of the Ni^{2+} macrodistribution (and molecular structure) in the pellets after drying, i.e., the stronger the adsorption to the surface after impregnation, the more uniform the Ni^{2+} distribution appeared to be after drying. Therefore, the use of chelating ligands such as ethylenediamine in preshaped catalyst preparation not only influences the molecular interactions with the support but also the final macrodistribution of the active species. This additional ingredient enables the preparation of either uniform or egg-shell Ni catalysts by controlling the ratios used in the precursor solutions.

Acknowledgment. The authors thank Dr. Tom Visser, Marjan Versluijs-Helder, and Alwies van der Heijden (Inorganic Chemistry and Catalysis group, Utrecht University) for their help in carrying out IR microspectroscopy, SEM-EDX analyses, and the preparation of modified alumina, respectively. The authors acknowledge financial support from ASPECT-ACTS.

References and Notes

(1) *Supported Metals in Catalysis*; Anderson, J. A., Fernandez Garcia, M., Eds.; Imperial College Press: London, 2005.

(2) *Preparation of Solid Catalysts*; Ertl, G.; Knozinger, H., Weitkamp, J., Eds.; Wiley-VCH: Weinheim, 1999.

(3) *Catalyst Preparation: Science and Engineering*; Regalbuto, J. R., Ed.; CRC Press: Boca Raton, 2007.

(4) de Jong, K. P. *Curr. Opin. Solid State Mater. Sci.* **1999**, *4*, 55.

(5) Neimark, A. V.; Kheifez, L. I.; Fenelonov, V. B. *Ind. Eng. Chem. Prod. Res. Dev.* **1981**, *20*, 439.

(6) Sietsma, J. R. A.; Meeldijk, J. D.; den Breejen, J. P.; Versluijs-Helder, M.; van Dillen, A. J.; de Jongh, P. E.; de Jong, K. P. *Angew. Chem., Int. Ed.* **2007**, *46*, 4547.

(7) Regalbuto, J. R.; Navada, A.; Shadid, S.; Bricker, M. L.; Chen, Q. *J. Catal.* **1999**, *184*, 335.

(8) Bourikas, K.; Kordulis, C.; Lycourghiotis, A. *Catal. Rev.* **2006**, *48*, 363.

(9) Heise, M. S.; Schwarz, J. A. *J. Colloid Interface Sci.* **1985**, *107*, 237.

(10) Lekhal, A.; Glasser, B. J.; Khinast, J. G. *Chem. Eng. Sci.* **2001**, *56*, 4473.

(11) Lekhal, A.; Glasser, B. J.; Khinast, J. G. *Chem. Eng. Sci*. **2004**, *59*, 1063.
(12) Van Dillen, A. J.; Terorde, R. J. A. M.; Lensveld, D. J.; Geus, J. W.; de Jong, K. P. *J. Catal*. **2003**, *216*, 257.
(13) (a) Bergwerff, J. A.; Visser, T.; Leliveld, B. R. G.; Rossenaar, B. D.; de Jong, K. P.; Weckhuysen, B. M. *J. Am. Chem. Soc*. **2004**, *126*, 14548. (b) Bergwerff, J. A.; van de Water, L. G. A.; Visser, T.; de Peinder, P.; Leliveld, B. R. G.; de Jong K. P.; Weckhuysen, B. M. *Chem. Eur. J*. **2005**, *11*, 4591. (c) van de Water, L. G. A.; Bergwerff, J. A.; Leliveld, B. R. G.; Weckhuysen, B. M.; de Jong, K. P. *J. Phys. Chem. B* **2005**, *109*, 14513.
(14) (a) van de Water, L. G. A.; Bergwerff, J. A.; Nijhuis, T. A.; de Jong, K. P.; Weckhuysen, B. M. *J. Am. Chem. Soc.* **2005**, *127*, 5024. (b) van de Water, L. G. A.; Bezemer, G. L.; Bergwerff, J. A.; Versluijs-Helder, M.; Weckhuysen, B. M.; de Jong, K. P. *J. Catal*. **2006**, *242*, 287. (c) Bergwerff, J. A.; Visser, T.; Weckhuysen, B. M. *Catal. Today* **2008**, *130*, 117.
(15) (a) Lysova, A. A.; Koptyug, I. V.; Sagdeev, R. Z.; Parmon, V. N.; Bergwerff, J. A.; Weckhuysen, B. M. *J. Am. Chem. Soc*. **2005**, *127*, 11916. (b) Bergwerff, J. A.; Lysova, A. A.; Espinosa-Alonso, L.; Koptyug, I. V.; Weckhuysen, B. M. *Angew. Chem., Int. Ed.* **2007**, *46*, 7224. (c) Bergwerff, J. A.; Lysova, A. A.; Espinosa-Alonso, L.; Koptyug I. V.; Weckhuysen, B. M. *Chem. Eur. J.* **2008**, *14*, 2363.
(16) Beale, A. M.; Jacques, S. D. M.; Bergwerff, J. A.; Barnes, P.; Weckhuysen, B. M. *Angew. Chem., Int. Ed.* **2007**, *46*, 8832.
(17) Salagre, P.; Fierro, J. L. G.; Medina, F.; Sueiras, J. E. *J. Mol. Catal. A* **1996**, *106*, 125.
(18) Negrier, F.; Marceau, E.; Che, M. *J. Phys. Chem. B* **2005**, *109*, 2836.
(19) Sun, K-Q.; Marceau, E.; Che, M. *Phys. Chem. Chem. Phys.* **2006**, *8*, 1731.
(20) Molina, R.; Centeno, M. A.; Poncelet, G. *J. Phys. Chem. B* **1999**, *103*, 6036.
(21) Baltes, M.; van der Voort, P.; Weckhuysen, B. M.; Ramachandra Rao, R.; Catana, G.; Schoonheydt, R. A.; Vansant, E. F. *Phys. Chem. Chem. Phys*. **2000**, *2*, 2673.
(22) Ryczkowski, J. *React. Kinet. Catal. Lett.* **1989**, *40*, 189.
(23) Pasieczna-Patkowska, S.; Ryczkowski J. *Appl. Surf. Sci.* **2007**, *253*, 5910.
(24) Schimpf, S.; Louis, C.; Claus, P. *Appl. Catal. A* **2007**, *318*, 45.
(25) Boudjay, S.; Lambert, J.-F.; Che, M. *J. Phys. Chem. B* **2003**, *107*, 651.
(26) Negrier, F.; Marceau, E.; Che, M.; de Caro, D. *C. R. Chimie* **2003**, *6*, 231.
(27) Boudjay, S.; Lambert, J.-F.; Che, M. *ChemPhysChem* **2004**, *5*, 1003.
(28) Dumond, F.; Marceau, E.; Che, M. *J. Phys. Chem. C* **2007**, *111*, 4780.
(29) Papageorgiou. P.; Price, D. M.; Gavriilidis, A.; Varma, A. *J. Catal.* **1996**, *158*, 439.
(30) Park, J.; Regalbuto, J. *J. Colloid Interface Sci.* **1995**, *175*, 239.
(31) Paoletti, P. *Pure Appl. Chem*. **1984**, *56*, 491.
(32) *Inorganic Electronic Spectroscopy*; Lever, A. B. P., Ed.; Elsevier Science B. V.: Amsterdam, 1987.
(33) Elkabouss, K.; Kacimi, M.; Ziyad, M.; Ammar, S.; Bozon-Verduraz, F. *J. Catal.* **2004**, *226*, 16.
(34) Flego, C.; O'Neil Parker, W., Jr. *Appl. Catal. A* **1999**, *185*, 137.
(35) Sun, M.; Nicosia, D.; Prins, R. *Catal. Today* **2003**, *86*, 173.
(36) *Metal Oxide Chemistry and Synthesis*; Jolivet, J.-P., Ed.; John Wiley & Sons Ltd.: Chinchester, 2000.
(37) Vigué, H.; Quintard, P.; Merle-Méjean, T.; Lorenzelli, V. *J. Eur. Cer. Soc.* **1998**, *18*, 305.
(38) Schwarz, J. A. *J. Catal*. **1990**, *122*, 202.
(39) Korah, J.; Spieker, W. A.; Regalbuto, J. R. *Catal. Lett.* **2003**, *85*, 123.
(40) Lambert, J-F.; Hoogland, M.; Che, M. *J. Phys. Chem. B* **1997**, *101*, 10347.
(41) De Bokx, P. K.; Wassenberg, W. B. A.; Geus, J. W. *J. Catal*. **1987**, *104*, 86.
(42) Vakros, J.; Bourikas, K.; Perlepes, S.; Kordulis, C.; Lycourghiotis, A. *Langmuir* **2004**, *20*, 10542.
(43) Roe, S. P.; Hill, J. O.; Magee, R. J. *Monatsh. Chem.* **1991**, *122*, 467.